Reactions of products from thermal degradation of PVC with nanoclusters of α-Fe_2O_3 (hematite)

Oday H. Ahmed, Mohammednoor Altarawneh, Zhong-Tao Jiang, Mohammad Al-Harahsheh, Bogdan Z. Dlugogorski

PII: S1385-8947(17)30582-X
DOI: http://dx.doi.org/10.1016/j.cej.2017.04.047
Reference: CEJ 16801

To appear in: *Chemical Engineering Journal*

Received Date: 22 December 2016
Revised Date: 16 March 2017
Accepted Date: 10 April 2017

Please cite this article as: O.H. Ahmed, M. Altarawneh, Z-T. Jiang, M. Al-Harahsheh, B.Z. Dlugogorski, Reactions of products from thermal degradation of PVC with nanoclusters of α-Fe_2O_3 (hematite), *Chemical Engineering Journal* (2017), doi: http://dx.doi.org/10.1016/j.cej.2017.04.047

Reactions of products from thermal degradation of PVC with nanoclusters of α-Fe_2O_3 (hematite)

Oday H. Ahmed[1, 2], Mohammednoor Altarawneh[1*],
Zhong-Tao Jiang[1], Mohammad Al-Harahsheh[3],
Bogdan. Z. Dlugogorski[1]

[1]School of Engineering and Information Technology, Murdoch University, Murdoch, WA 6150, Australia
[2]Department of Physics, College of Education, Al- Iraqia University, Baghdad, Iraq
[3]Department of Chemical Engineering, Jordan University of Science and Technology

*Corresponding author:

Email: M.Altarawneh@Murdoch.edu.au

Tel: +61-8-9360-7507

Abstract

Polyvinyl Chloride (PVC) plastics constitutes a large fraction of buildings, packaging and electronic devices, whereas, the annual emission electric arc furnace dust (EAFD) from steel manufacturing operations has recently peaked at nearly 6 Mt. Co-pyrolysis of PVC with EAFD currently represents a focal abatement technology for both categories of pollutants. However, despite of several experimental investigations; the mechanisms underlying interaction between EAFD and PVC remain largely speculative. Herein, we examine theoretically reactions of major products from thermal degradation of PVC with nanoclusters of iron (III) oxide, α-Fe_2O_3 (hematite) as a representative model for the various metal oxides in EAFD. The facile nature for the H-Cl bond fission over hematite is in line with experimental findings, pointing out to formation of iron chlorides from pyrolysis of Fe_2O_3-PVC mixtures. Interaction of selected chlorinated C_1-C_3 cuts with the hematite structure preferentially proceeds via a dissociative adsorption pathway. Results from this study shall be instrumental to understand, on a precise molecular basis, fixation of halogens on transitional metal oxides; a viabjjle thermal recycling approach for polymeric materials laden with halogenated constituents.

1. Introduction

Steel manufacturing facilities annually emit 4.3 – 5.7 Mt of electric arc furnace dust (EAFD) [1] . Designing an effective recycling methodology of EAFD has been a central research theme as it ensures the safeguard of the natural resources as well the environment. Due to the presence of heavy toxic metals such as Cr, Cd and Pb, EAFD imposes serious environmental and health concerns [2, 3]. For example, various metal oxides species in EAFD promote the formation of the notorious environmental persistent free radicals such as phenoxy [4]. The main elements of EAFD are zinc and iron, which vary in the range of 2-46% and 10-45%, respectively. These components mainly present in the form of zincite (ZnO), franklinite ($ZnFe_2O_4$), magnetite (Fe_3O_4), hematite (Fe_2O_3) and might also exist in small concentrations of hydrated zinc chloride [5, 6]. Thus, these high load of precious metals in EAFD have promoted a great deal of research aiming to extract metals from EAFD via both hydro-metallurgical and pyro-metallurgical techniques [2, 7]. The latter processes typical employ energy-intensive operations and necessitate complex clean-up methods [8]. This in turn reduces the economic feasibility of pyro-metallurgical operations. Similarly, applications of hydro-metallurgical procedures on an industrial scale are rather limited due to the accumulations of iron species in deployed acidic solutions that are very selective toward dissolution of zinc and lead [9, 10].

Co-pyrolysis of EAFD with halogen-containing materials has emerged as a promising synchronous recycling methodology for both resources [11]. The underlying derive of this approach relies on the profound fixation ability of halogenated species by metallic oxides constituents in EAFD [12, 14]. Polyvinyl chloride (PVC) represents

the largest fraction of the halogenated waste. Owing to superior chemical resistance and flame retardancy behavior, PVC is heavily used in electronic and electrical devices, construction materials, food packaging and household goods *etc* [15-18]. The global generation of PVC peaked at 61 Mt in 2013 and is projected to triple in 2021 [15]. Thermal recycling of PVC-containing waste plastic streams is not a viable option as it results in the generation of the hazardous polychlorinated dibenzo-*p*-dioxins and furan (PCDD/Fs) or dioxins for short [12, 19-21]. Effective Recycling of PVC truly rests on the ability to remove its chlorine content.

TGA-DSC studies on PVC and mixtures of PVC/metallic oxides provide insightful mechanistic insights into their decomposition behavior. Chemical analysis in GC/MS provides temperature-dependent product profiles of the decomposition products while XRD measurements track the change in the elemental composition of EAFD upon its co-pyrolysis with PVC [12, 22]. XRD patterns reported by Al-Harahsheh found that EAFD consists mainly of zincite (ZnO), franklinite ($ZnFe_2O_4$), magnetite (Fe_3O_4) and hematite (Fe_2O_3) [23]. Consensus of opinions from TGA profiles indicate that weight loss curve of pure PVC signifies two main peaks corresponding to elimination of HCl (around 200 ^oC) and fission of the carbon bonds in the PVC backbone (~ 360 ^oC). In a previous theoretical study [24], we have illustrated that, the common presence of defects in the structure of PVC, in terms of chlorines occupying tertiary positions, increases the reaction rate of the dehydrochlorination initial step (in reference to the ideal PVC structure encompassing secondary chlorines). Our previous kinetic analysis on HCl elimination from model compounds of PVC has also indicated that, rate constants for the dehydrochlorination step are independent of the length of the carbon chain [25].

The presence of EAFD during pyrolysis of PVC significantly reduces the activation energy of the first dehydrochlorination regime. The presence of EAFD enhances the mass loss of PVC in the first stage from 37% to nearly 80%. The additional mass loss was attributed to the formation of metal chlorides (mainly $ZnCl_2$ $PbCl_2$, $FeCl_2$, and $FeCl_3$,) [23].

It has been shown that ZnO, La_2O_3, Fe_2O_3 capture the emitted HCl from thermolysis of PVC [26]. The consumed chlorine transforms the metal oxides into metal chlorides. For instance, the addition of ferric oxide during thermal decomposition of PVC waste results in the formation of $FeCl_3$. These iron halides are consequently left in the residue after being subjected to water leaching [10]. Findings by Oleszek et al. has illustrated that, the co-combustion of Fe_2O_3 with tetrabromobisphenol (a majorly deployed brominated flame retardants) [27] assumes a similar role in suppressing formation of HBr and forms iron bromides [28].

An oxidation experiment by Masuda et al. [26] found that, the reaction of hematite (α-Fe_2O_3) with PVC significantly reduces the generation of HCl while enhancing the emission of gaseous products such as CO and CO_2 under various combustion conditions (in reference to neat PVC samples). Moreover, the yield of chlorobenzenes surprisingly increases upon introducing hematite. A plausible explanation is that the formed $FeCl_3$ mediates cyclization of fragmented polyenes into aromatic ring and acts as a chlorinating agent. Higher concentration of chlorobenzene boosts the char formation. More recently, Al-Harahsheh et al. [23] examined extraction of iron in EAFD by pyrolysing it with PVC. They showed that, between

25% and 56% of iron was recovered by leaching with boiling water, while the other remaining percentage represent magnetite and hematite.

Despite of detailed investigations into mixing of PVC with metal oxides over the last few years, the specific underlying mechanism of the reactions of HCl and other chlorinated C_1-C_6 cuts with hematite have remained poorly understood. In light of the importance of thermal recycling of halogenated fuels with hematite as an emerging abatement technology for both categories of pollutants, it is essential to understand the elemental processes governing interactions of halogenated species with metal oxides at a precise atomic scale. The fundamental objective is to design more efficient catalysts and to optimize the current deployed procedures. In particular, we aim to provide atomic-base insight into the detailed reaction pathways and to identify the key elementary steps that dictate the reaction rates. Many intermediates in the reaction PVC + Fe_2O_3 are expected to be highly transient nature and their presence in the system influences the overall yield of dechlorination process. Thermo-kinetic and mechanistic aspects of the investigated reactions could not be obtained by merely interpreting experimental results. These important aspects could only be obtained via carrying out accurate DFT calculations.

To this end, this manuscript reports a theoretical investigation into the reaction of HCl and selected chlorinated hydrocarbons with α-Fe_2O_3, as a model compound for metal oxides in EAFD. This study is part of our ongoing effort to investigate thermal recycling of halogenated fuels with Fe_2O_3 and other metallic oxides constituents in EAFD. In a recent study [24], we utilize a cluster model of α-Fe_2O_3 to investigate its reactions with a wide range of brominated alkanes, alkenes and aromatics.

Throughout the discussion, we pointed out to the difference in activation energies among the two halogenated systems. Herein, we attempt to map out reaction networks operating during the interaction of a cluster model of dehydrated α-Fe_2O_3 with both HCl and major products from the degradation of PVC. Findings from the current study can be useful to understand, on a precise molecular basis, the mechanisms of chlorine fixation on transitional metal oxides in the form of metal chlorides. Such knowledge finds direct application in the pursuit to design effective and viable recycling technologies for halogenated waste steam.

2. Computational method

Total energy and structural optimizations were carried out in the framework of the density functional theory (DFT) using the DMol^3 program package [29, 30]. Local Density Approximation (LDA) along the exchange-correlation of the Padrew and Wang (PAW) functional has been utilized in all calculations [31]. The theoretical methodology comprises a global cut-off of 3.6 Å and a double-polarized numeric basis set of DNP for all electrons [30]. The total energy achieves a tolerance of 1×10^{-6} Hartree. Final calculated energies were corrected via a dispersion correction term based on a methodology developed by Tkatchenko and Scheffle [32]. The complete LST/QST method locates transition states.

The obtained vibrational frequencies enable to estimate thermochemical parameters at elevated temperatures, from which Arrhenius rate parameters can be obtained. Reaction rate constants have been fitted to the Arrhenius equation over a temperature range of 300-1000 K based on the classical transition state theory [33]:

$$k\,(T) = A \exp\,(-E_a \,/\, RT)$$

Where A denotes preexponential factor, E_a signifies the activation energy, R stands for the gas constant (1.987 cal K^{-1} $mole^{-1}$) and T is the temperature in Kelvin [34].

For α-Fe_2O_3 (0001) surface calculations, A 3 × 3 × 1 Monkhorst-Pack κ-point scheme was used to perform the Brillouin zone integrations. The vacuum region between the adjacent slabs was set to 15 Å along the z-direction to reduce the interaction between the slabs. Throughout surface calculations, the top six layers as well as the adsorbed H and Cl atoms were allowed to relax, whilst the bottom two layers were kept fixed at their bulk positions.

3. Results and discussion

3.1. Hematite (α-Fe_2O_3) cluster

Hematite nanoparticles adapt a variety of crystallographic forms, for instance, alpha-hematite, beta-hematite and gamma-hematite. Among these different phases, α-Fe_2O_3 represents the most stable phase and assumes direct applications in many fields [35-38]. Hematite can be formed through oxidation of Fe_3O_4 at room temperature [39 ,40]:

$$O_2 + 4Fe_3O_4 \rightarrow 6Fe_2O_3$$

Herein, we adapt the $(Fe_2O_3)_{n=3}$ cluster utilized in our recent study [24] to model reactions of hematite with brominated motilities. Figure 1 depicts optimized structures of the α-Fe_2O_3 cluster. The optimized structure of α-Fe_2O_3 comprises three-fold coordinated iron atoms and two-fold coordinated oxygen atoms. To test the computational accuracy of the deployed α-Fe_2O_3 cluster, our calculated Fe-O interatomic distances, amount to 1.83/2.04 Å. These values reasonably match

analogous bulk values sourced from XANES spectra at 1.96/2.08 Å [41]. Our recently estimated Mayer bond orders and Hirshfeld charges provide detailed electronic analysis of the structure. Most importantly, the adapted α-Fe_2O_3 cluster features surface Fe-O bond that exists in the top layer of the most thermodynamically stable configuration of α-Fe_2O_3, namely the Fe_2O_3(001) facet [24]. In addition to well-defined surfaces, Fe_2O_3 in real systems also exists in the form the nanoparticles [42]. The presence of a particular surface termination in the nanostructures depends on its relative thermodynamic stability. For instance in a recent paper, we constructed a Wulff shape for copper bromide nanoparticles that incorporates more than one Miller index in its facets [43].

3.2. Dissociative adsorption of hydrogen chloride over α-Fe_2O_3 cluster

HCl signifies the initial and the most abundant product from decomposition of PVC. HCl typically accounts for nearly 55% of the total mass loss of PVC during its pyrolysis [44]. Thermodynamic calculations as well as pilot-scale measurements have unequivocally indicated that HCl is the most dominant chlorine species in the gas phase [45]. HCl is truly an inactive chlorinating agent on its own right; yet the so-called Deacon reaction readily transforms it into the active chlorinating agent of molecular chlorine (Cl_2) [46]. The growing experimental evidences from TGA-DSC profiles have elucidated that, evolved HCl from PVC converts Fe_2O_3 into $FeCl_{(n = 2\text{-}3)}$ [10]. Overall, we find that, HCl reaction with α-Fe_2O_3 proceeds in a very alike reaction network with that of HBr [24]. Yet, as expected higher bond dissociation energy (BDE) for H-Cl (103.2 kcal mol^{-1}) [45]. in reference to H-Br (87.1 kcal mol^{-1}) [47] dictates higher activation energies for the former system.

Figure 2 shows reactions encountered in the interaction of HCl with the α-Fe_2O_3 cluster. Physisorption of HCl on the α-Fe_2O_3 cluster generates the cluster-molecule adduct M1 that resides 10.6 kcal mol^{-1} below the separated reactants. In the M1 configuration, the H-Cl bond elongates by 7.1%, when compared with the equilibrium distance in the gaseous HCl molecule (1.39 Å). Dissociation of the adsorbed HCl molecule over Fe-O bond liberates 31.7 kcal mol^{-1} of excess energy and results in the formation of the M2 configuration. Breakage of the H-Cl bond along the reaction M1 → M2 demands a trivial activation energy of 10.3 kcal mol^{-1} via the transition structure TS1. This value slightly overshoots the analogous initial barrier in case of HBr; 8.2 kcal mol^{-1} [24]. The formed Fe-Cl bond length in the M2 structure amounts 2.30 Å, a value that reflects very well the analogous theoretical (2.17 Å) [48] value bond in bulk $FeCl_2$.

Conversion of Fe_2O_3 into $FeCl_{(n=2-3)}$ occur through two subsequent steps, further dissociative adsorption of HCl molecules on O-Fe linkages and the release of water molecules. Figure 2.b maps out these two chemical events. Decomposition of HCl on a neighboring O-Fe bond demands an activation energy of 12.1 kcal mol^{-1} and forms the structure of M4. In a subsequent step, the formation of M5 structure occurs through a slightly exothermic reaction of 5.5 kcal mol^{-1} and it necessitates a relatively sizable barrier of 27.9 kcal mol^{-1} characterized by TS3. This process produces adsorbed H_2O molecule via an intramolecular hydrogen transfer between the two hydroxyl groups. Inspection of the M5 structure illustrated in Figure 2.b reveals that, the ferryl Fe-OH_2 bond length (i.e., 2.20 Å) correlates very well with the corresponding distance (2.15 Å) for adsorbed water molecule on the hematite (0001) surface [49]. In the final step of the dissociative uptake of HCl, the water- iron

bonded molecule departs the cluster generating the oxychloride structure of M6 via an endothermic reaction of 21.4 kcal mol^{-1}. Clearly, the M6 structure presents a precursor for the transformation of Fe_2O_3 into iron chlorides. If the two-step process in Figure 2b continues, the hematite phase in EAFD is consumed into iron chlorides; in accord with the experimental observations.

The facile nature of mechanisms in Figure 2 indicates that, the formation of iron chlorides occurs simultaneously with the dehydrochlorination of PVC. This finding is in line with the experimental findings of Al-Harahsheh who observed a distinct reversal in the heat flow from an endothermic nature in pure PVC to an exothermic process in the presence of EAFD [23]. The exothermic event revealed by TGA-DSC data was attributed to the formation of new chemical new bonds leading to formation of metal chlorides. A significant 23% increase in the mass residue of the EAFD when co-pyrolysied with PVC was attributed to the fact that captured HCl does not leave EAFD as volatile iron chlorides [23]. In fact, evaporation of $FeCl_3$ along the reaction $Fe_2O_3 + 6HCl \rightarrow 2FeCl_3 + 3H_2O$ was found to be highly endothermic by ~ 32 kcal/mol at the temperature range of HCl release from PVC; i.e., 700 – 1000 K [10]. Nonetheless, iron volatilization in the form of iron chlorides was reported by Lee and Song who explained that, the rate of iron volatilization depends primarily on the heating rate where a negligible rate was observed at a heating rate below 5 K/min [12].

Table 1 lists estimated activation energies and pre-exponential *A* factor fitted in the temperature region of 300-1000 K for all reactions. Figure 3 depicts Arrhenius plots for the two HCl uptake reactions M1 → M2 and M4 → M5. In reference to the

corresponding HBr + Fe_2O_3 system [24], the first dissociative adsorption step in case of HCl is slower by factors of 113.2 and 68.4 at 500 K and 750 K; respectively. Thus, it is inferred, that chlorination of Fe_2O_3 by HCl to be slower than its bromination by HBr. Nonetheless, both halogenation mechanism adapt similar reaction pathways.

It is very-well documented that energies obtained from deploying a cluster model maybe sensitive to the edge effects when contrasted with periodic systems [50]. However, reactions of PVC constituents with the Fe_2O_3 model occur on the catalytic active sites; that are surface Fe-O bonds which are well represented in the cluster model. In order to provide a structural and energy comparison between a cluster versus a periodic surface models, we utilize a surface model of the α-Fe_2O_3 (0001) termination to investigate the first reaction step entailing HCl molecule and contrasted obtained values with corresponding results obtained from the cluster model. Figure 4 presents energies and structures for the first step in the HCl + Fe_2O_3 interaction. The following remarks summarise the satisfactory agreement between the two models

1- As illustrated in Figure 4, the H-Cl bond of $M1_{Surface}$ configuration is elongated by 6.9% in comparison with the equilibrium distance in the gaseous HCl molecule (1.39 Å). This reasonably corresponds with our finding from the cluster model (i.e. 7.1%).

2- In the dissociative structure ($M2_{Surface}$), the Fe-Cl bond length amounts 2.35 Å, a value that reflects very well the analogous value in the cluster model, i.e. 2.30 Å.

3- Physisorption and chemisorption energies for the reaction of HCl on the α-Fe_2O_3 (00001) surface (-9.1 and -36.2 kcal mol^{-1}) agree well with the values obtained over the cluster (i.e. -10.6 and -42.3 kcal mol^{-1}).

3.3. Degradation mechanisms of organohalogens

Breakages of carbon linkages in PVC during its pyrolysis produce a wide range of chlorinated compounds [15, 20, 27, 51]. In an analogy to our recent study on thermal recycling of brominated flame retardants using α-Fe_2O_3 [24], we study the interaction of hematite nanoclusters with various chlorine model molecules; namely (Chloroethene (CH_2CHCl), 1-chloro-1-propene (C_3H_5Cl), chloroethane (CH_3CH_2Cl) and 2-chloropropane (C_3H_7Cl)). These compounds serve as a good representation of chlorinated structural entities stemmed from thermal decomposition of PVC; with corresponding carbon – chlorine BDE falling in the narrow range of 84.6 - 91.2 kcal mol^{-1} [47, 52].

Reaction of chlorinated alkanes and alkenes with α-Fe_2O_3 cluster can take place through two possible pathways: (i) direct HCl elimination featured with high energy barriers; (ii) low-energy dissociative addition that is followed by a β-hydride elimination step; thereby forming olefins. Lewis acid–base pairs in metal oxides function as potent catalysts for the cleavage of carbon-halogen bonds with greater selectivity if compared with carbon-hydrogen bonds [53, 54]. In this section, we assess the catalytic capacity of α-Fe_2O_3 toward dehydrochlorination of the selected chlorinated C_2-C_3 cuts with the aim to illustrate chemical phenomena encountered in the co-pyrolysis of EAFD with fragments of PVC.

Figure 5 shows both direct elimination and dissociative addition reactions for the catalytic decomposition of vinyl chloride, 1-propenyl chloride, ethyl chloride and 2-propyl chloride on the α-Fe_2O_3 cluster. In the first step of these reactions, an initial cluster–molecule adduct initiates the Lewis acid–base reaction between α-Fe_2O_3

cluster and the considered organohalogen molecules. In the initial physisorbed states, carbon–chlorine bonds in the chloroethene, 1-chloro-1-propene, chloroethane and 2-chloropropane are elongated by 23.5%, 5.6%, 6.5% and 15.7%, respectively when compared with the equilibrium distances of their parent gas phase molecules.

α-Fe_2O_3 cluster displays effectiveness towards dissociative addition pathway in which the surface Fe-O linkages participate in the activation of the C–Cl bond in the first step. Despite of our best efforts, no transition states could be located for the rupture of the C-Cl bonds in chloroethane and 2-chloropropane, while the process proceeds via trivial barriers of 6.5 kcal mol^{-1} (TS5 in Figure 5.A) and at 14.0 kcal mol^{-1} (TS7A in Figure 5.B) for chloroethene and 1-chloro-1-propene, correspondingly. The next step is the activation of C–H bond followed via a β(H)-hydride transfer to an oxygen site to form an olefin. The β-hydride elimination steps require sizable activation energies varying between 69.2 kcal mol^{-1} for the desorption of CH_3CHCH_2 molecule (TS11B) to 87.2 kcal mol^{-1} required to form a CH_3CCH molecule (TS7B) as shown in panels D and B in Figure 5, respectively. Generally, barrier for the desorption of stable molecules via the β(H)-hydride transfer rests not only on the strength of the dissociated C-H bond, but as well on the strength of the O-C bonds [47].

Considering the direct HCl elimination pathway, Fe-O bonds significantly reduces barriers for the dehydrochlorination corridor in reference to the uncatalyzed analogous gas phase process. For example, the formation of ethene through TS8 requires a barrier energy of 36.6 kcal mol^{-1}. This is significantly lower than that for the homogenous HCl elimination from chloroethane, i.e. 57.5 kcal mol^{-1} [55].

Careful examinations of reactions in Figure 5, provides three important indications: (i) elimination corridors systematically require higher barrier energies in the range of 36.6– 59.9 kcal mol^{-1} than dissociative addition formation, whose reaction barrier reside in the range of 6.5 – 14.0 kcal mol^{-1}, (ii) while barriers for the direct elimination routes are significantly higher than dissociative addition channels, barriers for the subsequent β-hydrogen transfer incur overall barriers that are comparable with the barriers of the direct elimination pathways, and (iii) dissociative addition routes undergo the S_N2 category of mechanism, whilst the direct elimination routes undergo the $E2$ mechanisms (bimolecular elimination) similar to the analogous mechanism prevailing in the dehydration of ethanol over Al_2O_3 [56].

Considering the dissociative adsorption channel as a two-step mechanism affording the products of the direct elimination pathway, the dissociative addition channel is expected to predominate the direct elimination route for chloroethene (30.3 kcal mol^{-1} versus 59.9 kcal mol^{-1}) whereas the latter should prevail over the former for chloroethane (36.6 kcal mol^{-1} versus 40.8 kcal mol^{-1}). Both mechanisms incur very similar overall activation barriers for 1-chloro-1-propene (60.2 kcal mol^{-1} versus 59.9 kcal mol^{-1}). Nonetheless, such small difference most likely resides within the expected accuracy margin of the adapted theoretical methodology.

Obtained barriers for the direct elimination pathway seem to positively correlate with the carbon-chlorine BDEs. For instance, as shown from panel C and D in Figure 5, the HCl elimination channel in case of chloroethane (C-Cl BDE = 84.2 kcal mol^{-1}) and 1-chloro-propene (C-Cl BDE =88.6 kcal mol^{-1}) proceeds via very distinct barriers of 36.6 kcal mol^{-1} and 50.0 kcal mol^{-1}; in that order.

Figure 6 shows the variation in the rate constant of the two possible pathway reactions between 300 and 1000 K. Reaction rate constants for the two steps in the dissociative adsorption route has been estimated with considering the physisorbed state as the initial reactant. Based on values in Figure 6, the dissociative addition pathway predominates the direct elimination channel for the formation of both ethyne as well as propene from chloroethene and 2- chloropropane, respectively. Small chlorine-free hydrocarbons were detected in the experiments of Al-Harahsheh et al. [23]. The formation of these alkynes/alkenes support the occurrence of the demonstrated dehydrochlorination. On the other hand, the direct elimination pathway represents the only possible route to yield ethene from dehydrohalogenation of chloroethane on the α-Fe_2O_3 cluster. For instance, in the dissociative addition pathway, the rate reaction constant for chloroethane is less sensitive to the temperature comparing to that for chloroethene. When contrasted with the slow homogenous dehydrochlorination pathway in the gas phase [55], the catalytic-assisted HCl removal demonstrated herein indicates that, iron oxides serve as active catalysts in producing clean olefins streams from chlorinated alkanes; in analogy to the well-documented role of alumina and other metal oxides[57, 59] .

3.4. Reaction of α-Fe_2O_3 cluster with chlorobenzene and 2-chlorophenol

Condensation of polyenes produced from PVC yields appreciable concentrations of benzene and other aromatic cyclic compounds [27]. As conveyed earlier, the presence of EAFD promotes the formation of chlorobenzene; presumably mediated by $FeCl_3$. If oxygen exists during thermal degradation of PVC, formed chlorobenzene could be readily oxidized into chlorophenols [60]. Both groups act as direct building blocks for the synthesis of dioxins. Thus, it is insightful to assess the chlorination of

chlorobenzenes and chlorophenols over hematite nanoclusters. Herein, we have investigated the interaction of α-Fe_2O_3 cluster with 1-chlorobenzene and 2-chlorophenol as model compounds for these groups of chlorinated aromatics.

Figure 7.a shows that, interaction of chlorobenzene with the α-Fe_2O_3 cluster forms the M20 moiety in a considerable exothermic reaction of -44.8 kcal mol^{-1}. Fission of the strong aromatic C-Cl bond (95.5 kcal mol^{-1}) via TS12 occurs through an activation barrier of 15.4 kcal mol^{-1}. This value noticeably exceeds the analogous barrier in case of bromobenzene by 4.1 kcal mol^{-1}. Obviously, a weaker aromatic C-Br bond by almost 12.0 kcal mol^{-1} [52] derives this noticeable difference in activation energy for the carbon-halogen bond fission. The formed phenyl ring in the M20 structure is strongly bonded with two neighboring iron atoms. Thus it is highly unlikely for phenyl to desorb. Fragmentation into C_2H_2 molecules and the coverage of Fe_2O_3 surfaces with carbonaceous layers may control the fate of the phenyl adduct. Another plausible channel is the cross-linking of two adjacent phenyls into a biphenyl molecule. Subsequent reactions following the formation of an adsorbed phenyl radical on the hematite cluster warrants further investigation.

Figure 7.b reports the scission of the two weakest bonds in the 2-chlorophenol molecule over the α-Fe_2O_3 cluster; the hydroxyl O-H bond (89.0 kcal mol^{-1}) [52] and C-Cl bond (95.5 kcal mol^{-1}) [52]. Fission of aromatic C-Cl bond demands a significantly lower activation barrier in reference to the rupture of the fission of the phenol's O-H bond (15.0 versus 34.8 kcal mol^{-1}). It follows that interaction of the chlorophenols solely yields hydroxylated phenyl-type radicals; rather than phenoxy radicals. Recent theoretical investigations have recently illustrated mechanisms for the

homogenous generation of PCDD/Fs from phenyl-type radicals [61]. The weakly adsorbed 2-OH-phenyl radical in the M23 configuration may undergo through Langmuir–Hinshelwood (LH) and Eley–Rideal (ER) mechanisms [46, 62] to yield PCDD/Fs. Therefore, while Fe_2O_3 assumes profound chlorine fixation ability, it could also facilitate generation of direct precursors for the formation of dioxins [63, 64]. The dual role of Fe_2O_3 in dechlorination reactions of aromatics and mediating formation of dioxins require further detailed examination.

4. Conclusions and Future Directions

By performing accurate DFT calculations, we have systematically surveyed initial reactions involving a cluster model of α-Fe_2O_3 and major chlorine-bearing species from the fragmentation of PVC. We have demonstrated that, successive uptake of HCl molecules followed by water elimination lead to the formation of a precursor for iron chlorides. Owing to stronger carbon-chlorine bonds in the considered molecules, their dissociative addition corridors assume higher activation barriers in comparison with their brominated counterparts. We found that interaction of hematite nanoclusters with 2-chlorophenol to preferentially form an OH-phenyl radical (via carbon-chlorine bond rupture) rather than 2-chlorophenoxy radical (via O-H bond fission). While results from this study provide useful information pertinent to the considered dehydrohalogenation reactions facilitated by hematite, it also suggests that further future work is needed to address some intriguing questions in regard to:

1- The role of Fe_2O_3 as a catalysis in the surface-mediated formations of PCDD/Fs. Relevant experimental studies on co-pyrolysis of PVC with EAFD

have mainly addressed the merits of metal oxides as chlorine fixation agents with little emphasis on the likely potential to generate dioxin compounds.

2- A principal aim for the co-pyrolysis of PVC with EAFD is to extract its high load of zinc content. Zinc in EAFD mainly exists in the form of $ZnFe_2O_4$. It is assumed that formation of the leachable zinc chloride occurs through migration of chlorine from iron chlorides into $ZnFe_2O_4$. It will be informative to examine this mechanistic hypothesis against direct plausible dissociation of HCl on Zn-O bonds.

5. Acknowledgements

This work has been supported by Australia and Pawsey Supercomputing Centre in Perth, Australian Research Council (ARC) and the National Computational Infrastructure (NCI). O.A thanks the higher committee for education development in Iraq (HCED) for the award of a postgraduate scholarship.

References

[1] N. Leclerc, E. Meux and J. M. Lecuire, Hydrometallurgical extraction of zinc from zinc ferrites, Hydrometallurgy 70 (2003) 175-183.

[2] T. Suetens, B. Klaasen, K. V. Acker and B. Blanpain, Comparison of electric arc furnace dust treatment technologies using exergy efficiency, J. Clean. Prod. 65 (2014) 152-167.

[3] G. Assis, Emerging pyrometallurgical processes for zinc and lead recovery from zinc-bearing waste materials, Mintek, 1998.

[4] N. W. Assaf, M. Altarawneh, I. Oluwoye, M. Radny, S. M. Lomnicki and B. Z. Dlugogorski, Formation of environmentally persistent free radicals on α-Al_2O_3, Environ.Sci. Technol. 50 (2016) 11094-11102.

[5] T. Havlík, B.V. e. Souza, A.M. Bernardes, I.A.H. Schneider and A. Miškufová, Hydrometallurgical processing of carbon steel EAF dust, J. Hazard. Mater. 135 (2006) 311-318.

[6] D.K. Xia, and C.A. Picklesi, Microwave caustic leaching of electric arc furnace dust, Miner. Eng. 13 (2000) 79-94.

[7] J. Antrekowitsch and H. Antrekowitsch, Hydrometallurgically recovering zinc from electric arc furnace dusts, J. Min. Met. Mater. Soc. 53 (2001) 26-28.

[8] M. K. Jha, V. Kumar and R. Singh, eview of hydrometallurgical recovery of zinc from industrial wastes, Resour. Conserv. Recycl. 33 (2001) 1-22.

[9] G. Orhan, Leaching and cementation of heavy metals from electric arc furnace dust in alkaline medium, Hydrometallurgy 78 (2005) 236-245.

[10] M. Al-Harahsheh, A. Al-Otoom, L. Al-Makhadmah, I. E. Hamilton, S. Kingman, S. Al-Asheh and M. Hararah, Pyrolysis of poly (vinyl chloride) and-electric arc furnacedust mixtures, J. Hazard. Mater. 299 (2015) 425-436.

[11] J. Korpas, V. Slovák and K. Wichterle, Waste poly (vinyl chloride) pyrolysis with hydrogen chloride abatement by steelmaking dust, Chemical Papers 70 (2016) 926-932.

[12] G. S. Lee and Y. J. Song, Recycling EAF dust by heat treatment with PVC, Miner. Eng. 20 (2007) 739-746.

[13] B. Gui, Y. Qiao, D. Wan, S. Liu, Z. Han, H. Yao and M. Xu, P. Nascent tar formation during polyvinylchloride (PVC) pyrolysis, Combust. Inst. 34 (2013) 2321-2329.

[14] M. Sarker and M. M. Rashid, Waste plastics mixture of polystyrene and polypropylene into light grade fuel using Fe_2O_3 catalyst Int. J. Renew. Energy Technol. Res. 2 (2013) 17-28.

[15] J. Yu, L. Sun, C. Ma, Y. Qiao and H. Yao, Thermal degradation of PVC: a review, Waste manage. 48 (2016) 300-314.

[16] G. Sivalingam, R. Karthik and G. Madras, Effect of metal oxides on thermal degradation of poly (vinyl acetate) and poly (vinyl chloride) and their blends, Ind. Eng. Chem. Res. 42 (2003) 3647-3653.

[17] G. Plotnikova, K. Kuznetsov, S. Malysheva, V. Udilov, V. Y. Seleznev, N. Belogorlova and V. Kuimov, Int. J. Polym. Sci. Tech. 37 (2010) T29.

[18] H. Wang, H. Wang, Z. Guo, S. Qi and C. Tian, Flame retardant property of Sb_2O_3/SnO_2 and their synergism in flexible PVC, J. Fire Sci. 24 (2006) 195-210.

[19] T. Katami, A. Yasuhara, T. Okuda and T. Shibamoto, Formation of PCDDs, PCDFs, and coplanar PCBs from polyvinyl chloride during combustion in an incinerator, Environ. Sci. Technol. 36 (2002) 1320-1324.

[20] C. Huggett and B. C. Levin, Toxicity of the pyrolysis and combustion products of poly (vinyl chlorides): a literature assessment, Fire Mater. 11 (1987) 131-142.

[21] P. Carty, E. Metcalfe and T. Saben, Thermal analysis of plasticised PVC containing flame retardant/smoke suppressant inorganic and organometallic iron compounds Fire safety J. 17 (1991) 45-56.

[22] T. Iida and K. Gotō, Investigations on poly (vinyl chloride). III. Effects of metal oxides upon thermal decomposition of poly (vinyl chloride), J. Polym. Sci. Polym. Chem. Ed. 15 (1977) 2427-2433.

[23] M. Al-Harahsheh, S. Kingman, L. Al-Makhadmah and I. E. Hamilton, Microwave treatment of electric arc furnace dust with PVC: Dielectric characterization and pyrolysis-leaching, J. Hazard. Mater. 274 (2014) 87-97.

[24] M. Altarawneh, O. H. Ahmed, Z. T. Jiang and B. Z. Dlugogorski, Thermal recycling of brominated flame retardants with Fe_2O_3, J. Phys. Chem. A. 120 (2016) 6039-6047

[25] N. Ahubelem, M. Altarawneh and B. Dlugogorski, Kinetic and mechanistic study into emission of HCl in fires of PVC (2013) 371-380

[26] Y. Masuda, T. Uda, O. Terakado and M. Hirasawa, Pyrolysis study of poly (vinyl chloride)–metal oxide mixtures: quantitative product analysis and the chlorine fixing ability of metal oxides J. Anal. Appli. Pyrol. 77 (2006) 159-168.

[27] R. Font, A. Galvez, J. Molto, A. Fullana and I. Aracil, Formation of polychlorinated compounds in the combustion of PVC with iron nanoparticles Chemosphere 78 (2010) 152-159.

[28] S. Oleszek, M. Grabda, E. Shibata and T. Nakamura, Study of the reactions between tetrabromobisphenol A and PbO and Fe_2O_3 in inert and oxidizing atmospheres by various thermal methods Thermochim. Acta. 566 (2013) 218-225.

[29] B. Delley, From molecules to solids with the DMol 3 approach, J. Chem. Phys. 113 (2000) 7756-7764.

[30] B. Delley, An all-electron numerical method for solving the local density functional for polyatomic molecules J. Chem.Phys. 92 (1990) 508-517.

[31]J. P. Perdew and K. Burke, Comparison shopping for a gradient-corrected density functional Int. J. Quantum chem. 57 (1996) 309-319.

[32] A. Tkatchenko and M. Scheffler, Accurate molecular van der Waals interactions from ground-state electron density and free-atom reference data Phys. Rev. Lett. 102 (2009) 073005.

[33] K. J. Laidler and M. C. King, The development of transition-state theory J. phys. chem. 87 (1983) 2657-2664.

[34] F. A. Carroll, Perspectives on structure and mechanism in organic chemistry, John Wiley & Sons, 2011.

[35]C. S. Lewis, L. Torres, J. T. Miyauchi, C. Rastegar, J. M. Patete, J. M. Smith, S. S. Wong and S. E. Tsirka, Absence of cytotoxicity towards microglia of iron oxide (α-Fe_2O_3) nanorhombohedra Toxicology research 5 (2016) 836-847.

[36] G. Tong, J. Guan and Q. Zhang, Goethite hierarchical nanostructures: Glucose-assisted synthesis, chemical conversion into hematite with excellent photocatalytic properties Mater. Chem. Phys. 127 (2011) 371-378.

[37] A. Erlebach, H. D. Kurland, J. Grabow, F. A. Muller and M. Sierka, Structure evolution of nanoparticulate Fe_2O_3, Nanoscale 7 (2015) 2960-2969.

[38] S. Yang, X. Song, P. Zhang and L. Gao, Heating-rate-induced porous α-Fe_2O_3 with controllable pore size and crystallinity grown on graphene for supercapacitors ACS Appl. Mater. Interfaces. 7 (2015) 75-79.

[39] B. Monsen, S. Olsen and L. Kolbeinsen, Scand. Kinetics of magnetite oxidation J. Metal. 23 (1994) 74-80.

[40] E. R. Monazam, R. W. Breault and R. V. Siriwardane, Kinetics of magnetite (Fe3O4) oxidation to hematite (Fe_2O_3) in air for chemical looping combustion Ind. Eng. Chem. Res. 53 (2014) 13320-13328.

[41] L. X. Chen, T. Liu, M. C. Thurnauer, R. Csencsits and T. Rajh, Fe_2O_3 nanoparticle structures investigated by X-ray absorption near-edge structure, surface modifications, and model calculations J. Phys. Chem. B. 106 (2002) 8539-8546.

[42] M. Kurmoo, J. L. Rehspringer, A. Hutlova, C. D'Orléans, S. Vilminot, C. Estournès, and D. Niznansky, Formation of nanoparticles of ε-Fe_2O_3 from yttrium iron garnet in a silica matrix: An unusually hard magnet with a Morin-like transition below 150 K Chem. Mater. 17 (2005) 1106-1114.

[43] M. Altarawneh, A. Marashdeh and B.Z. Dlugogorski, Phys. Chem. Chem. Phy. 17 (2015) 9341-9351.

[44]I. C. McNeill, L. Memetea and W. J. Cole, A study of the products of PVC thermal degradation Polym. Degrad. Stab. 49 (1995). 181-191.

[45] E. Wikström, S. Ryan, A. Touati, M. Telfer, D. Tabor and B. K. Gullett, Importance of chlorine speciation on de novo formation of polychlorinated dibenzo-p-dioxins and polychlorinated dibenzofurans Environ. Sci. Technol. 37 (2003) 1108-1113.

[46] M. Altarawneh, B. Z. Dlugogorski, E. M. Kennedy and J. C. Mackie, Mechanisms for formation, chlorination, dechlorination and destruction of polychlorinated dibenzo-p-dioxins and dibenzofurans (PCDD/Fs), Prog. Energy Combust Sci. 35 (2009) 245-274.

[47] S. J. Blanksby and G. B. Ellison, Bond dissociation energies of organic molecules Acc. Chem. Res. 36 (2003) 255-263.

[48] T. Liu, L. Xue, X. Guo, Y. Huang and C. Zheng, Environ. DFT and Experimental Study on the Mechanism of Elemental Mercury Capture in the Presence of HCl on α-Fe_2O_3 (001), Sci. Technol. 50 (2016) 4863-4868.

[49] S. Yin and D. E. Ellis, H_2O adsorption and dissociation on defective hematite (0001) surfaces: A DFT study. Surf. Sci. 602 (2008) 2047-2054.

[50] M. Petrantoni, A. Hemeryck, J.M. Ducéré, A. Estève, C. Rossi, M.D. Rouhani, D. Estève and G. Landa, Periodic boundary versus quantum cluster approaches in the simulation of a nanoenergetic metallic model-system: Ni/Al (111) surface reactions J. Phys. Chem. Solids. 71 (2010) 130-133.

[51] R. Miranda, H. Pakdel, C. Roy, H. Darmstadt and C. Vasile, Vacuum pyrolysis of PVCII: Product analysis, Polym. Degrad. Stab. 66 (1999) 107-125.

[52] Y.-R. Luo, Handbook of bond dissociation energies in organic compounds, CRC press, 2002.

[53] R. Wischert, C. Copéret, F. Delbecq and P. Sautet, Optimal Water Coverage on Alumina: A Key to Generate Lewis Acid–Base Pairs that are Reactive Towards

the C- H Bond Activation of Methane Angew. Chem. Int. Ed. 50 (2011) 3202-3205.

[54] A. Comas-Vives, M. Schwarzwälder, C. Copéret and P. Sautet, Carbon–Carbon Bond Formation by Activation of CH_3F on Alumina J. Phys. Chem. C. 119 (2015) 7156-7163.

[55] N. Ahubelem, M. Altarawneh and B. Z. Dlugogorski, Dehydrohalogenation of ethyl halides Tetrahedron Lett. 55 (2014) 4860-4868.

[56] S. Roy, G. Mpourmpakis, D.Y. Hong, D. G. Vlachos, A. Bhan and R. Gorte, Mechanistic Study of Alcohol Dehydration on γ-Al_2O_3, ACS Catalysis. 2 (2012) 1846-1853.

[57] W. Khaodee, N. Tangchupong, B. Jongsomjit, P. Praserthdam and S. Assabumrungrat, A study on isosynthesis via CO hydrogenation over ZrO_2-CeO_2 mixed oxide catalysts Catal. Commun. 10 (2009) 494-501.

[58] R. C. R. Neto and M. Schmal, Synthesis of CeO_2 and $CeZrO_2$ mixed oxide nanostructured catalysts for the iso-syntheses reaction Appl. Catal. A: General. 450 (2013) 131-142.

[59] Z. Wu, C. Li, Z. Wei, P. Ying and Q. Xin FT-IR spectroscopic studies of thiophene adsorption and reactions on Mo_2N/γ-Al_2O_3 catalysts, J. Phys. Chem. B. 106 (2002) 979-987.

[60] P. M. Sommeling, P. Mulder and R. Louw, Formation of PCDFs during chlorination and oxidation of chlorobenzene in chlorine/oxygen mixtures around 340 C Chemosphere. 29 (1994). 2015-2018.

[61] Y. Zhang, D. Zhang, J. Gao, J. Zhan and C. Liu, New understanding of the formation of PCDD/Fs from chlorophenol precursors: a mechanistic and kinetic study J. Phys. Chem. A. 118 (2014) 449-456.

[62] Q. Sun, M. Altarawneh, B. Z. Dlugogorski, E. M. Kennedy and J. C. Mackie, Catalytic effect of CuO and other transition metal oxides in formation of dioxins: theoretical investigation of reaction between 2, 4, 5-trichlorophenol and CuO, Environ. Sci. Technol. 41 (2007) 5708-5715.

[63] M. Altarawneh, D. Carrizo, A. Ziolkowski, E.M. Kennedy, B.Z. Dlugogorski, and J.C. Mackie, Pyrolysis of permethrin and formation of precursors of polychlorinated dibenzo-p-dioxins and dibenzofurans (PCDD/F) under non-oxidative conditions Chemosphere. 74 (2009) 1435–1443.

[64] M. Altarawneh, M. W. Radny, P. V. Smith, E. M. Kennedy, J. C. Mackie, and B. Z. Dlugogorski, Adsorption of chlorophenol on the Cu (111) surface: A first-principles density functional theory study Appl. Surf. Sci. 254 (2008) 4218- 4224

Table 1: Kinetic parameters of reactions fitted in the temperature range of 300-1000 K.

Species	Reaction	A (s^{-1})	Ea (kcal mol^{-1})
Hydrogen chloride	M 1→ M2	3.18×10^{10}	7.9
	M3 → M4	6.65×10^{10}	8.3
	M5 → M6	9.27×10^{10}	22.9
Chloroethene	M7 → M9	3.00×10^{11}	5.8
	M7 → M8 direct elimination	1.12×10^{11}	46.5
	M7 → M8 dissociative adsorption	8.22×10^{10}	73.9
1-Chloro-1-propene	M10 → M12	3.32×10^{11}	13.5
	M10 → M11 direct elimination	3.06×10^{10}	53.1
	M10 → M11 dissociative adsorption	4.82×10^{10}	76.8
Chloroethane	M13 → M14 direct elimination	3.43×10^{9}	30.9
	M13 → M14 dissociative adsorption	1.42×10^{11}	65.1
2-Chloropropane	M16 → M17 direct elimination	2.84×10^{10}	43.8
	M16 → M17 dissociative adsorption	1.77×10^{12}	61.1
Chlorobenzene	M19 → M20	1.99×10^{12}	14.3
2- Chlorophenol	M21 → M23	5.14×10^{15}	20.3
	M21 → M22	7.19×10^{15}	34.2

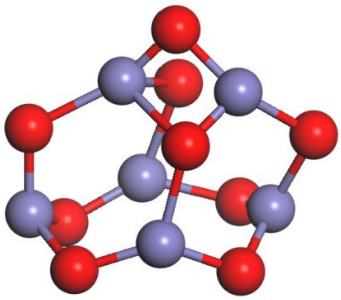

Figure 1: Optimized structure of Hematite (α-Fe_2O_3) cluster. Blue spheres denote iron atoms and red spheres signify oxygen atoms. This code of colours applies to all Figures.

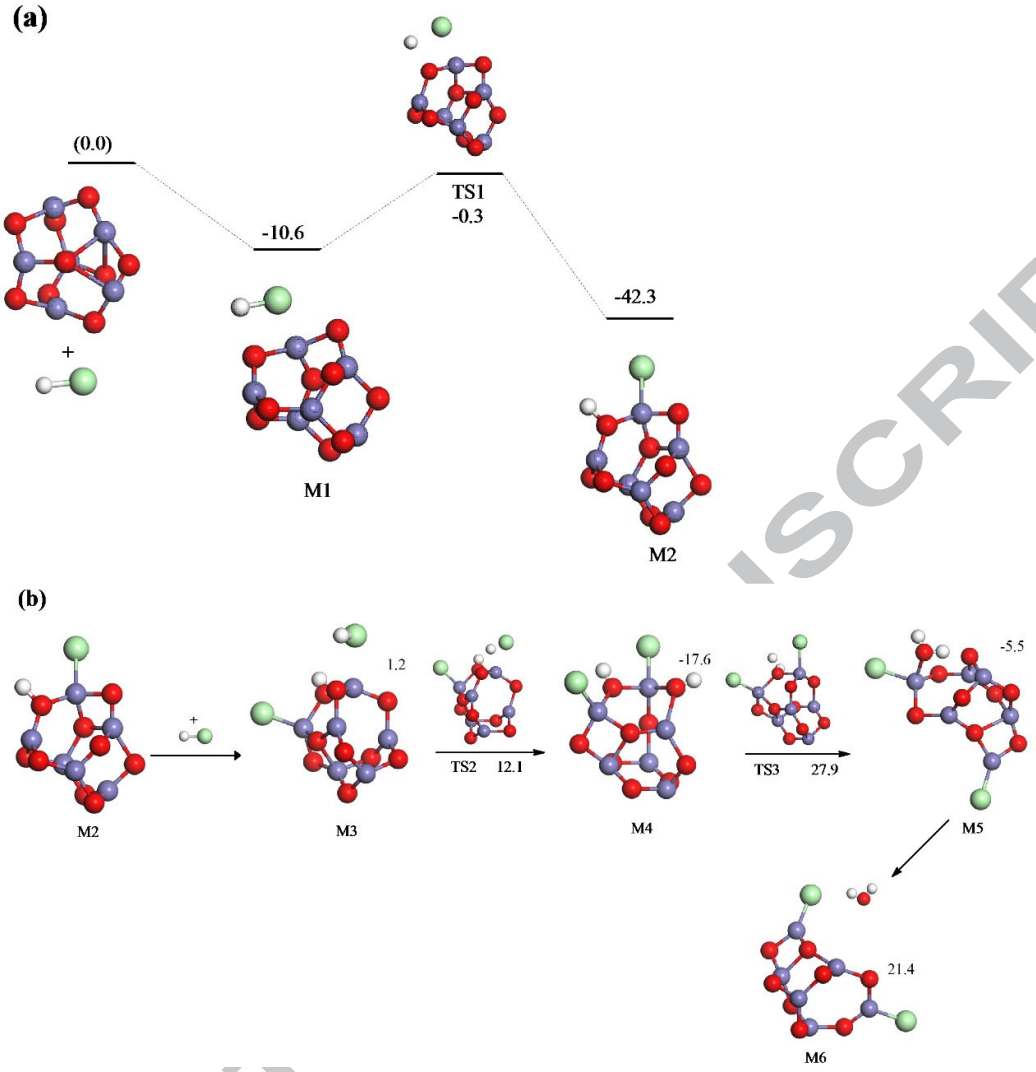

Figure 2: Reaction mechanism for HCl molecule and the hematite (α-Fe_2O_3) cluster. Values are in kcal mol^{-1} with respect to the initial reactant in (a) and to reactants in each step in (b). Large green spheres denote chlorine atoms and white spheres signify hydrogen.

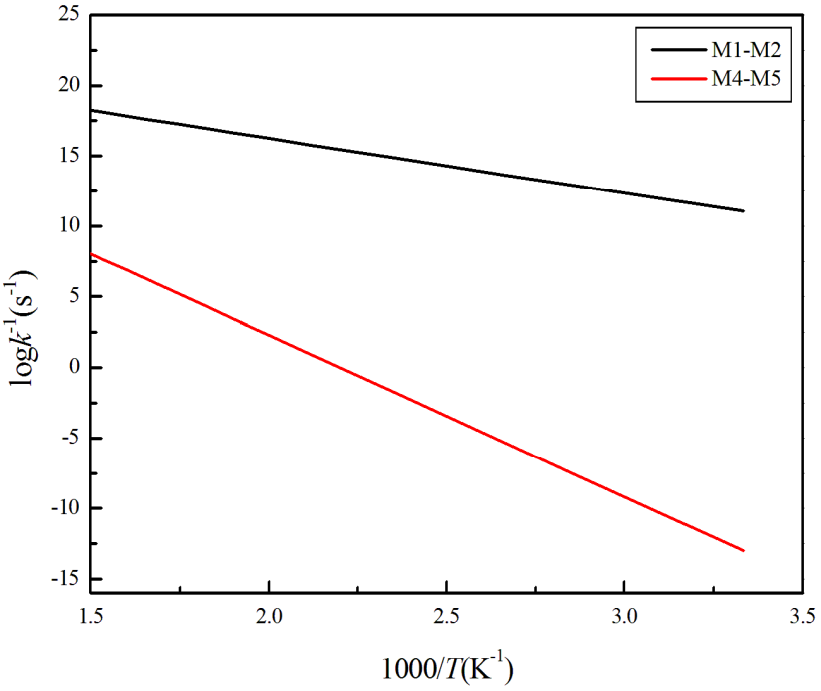

Figure 3: Arrhenius plots for reactions between the hematite (α-Fe_2O_3) cluster and HCl molecules.

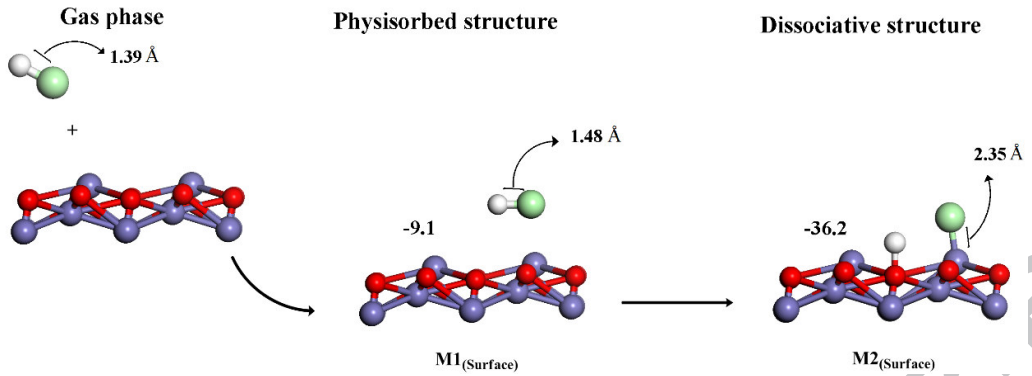

Figure 4: Reaction mechanism for HCl molecule and the hematite (α-Fe_2O_3) surface. Values are in kcal mol^{-1} with respect to the initial reactant. Only the first two Fe layers are shown.

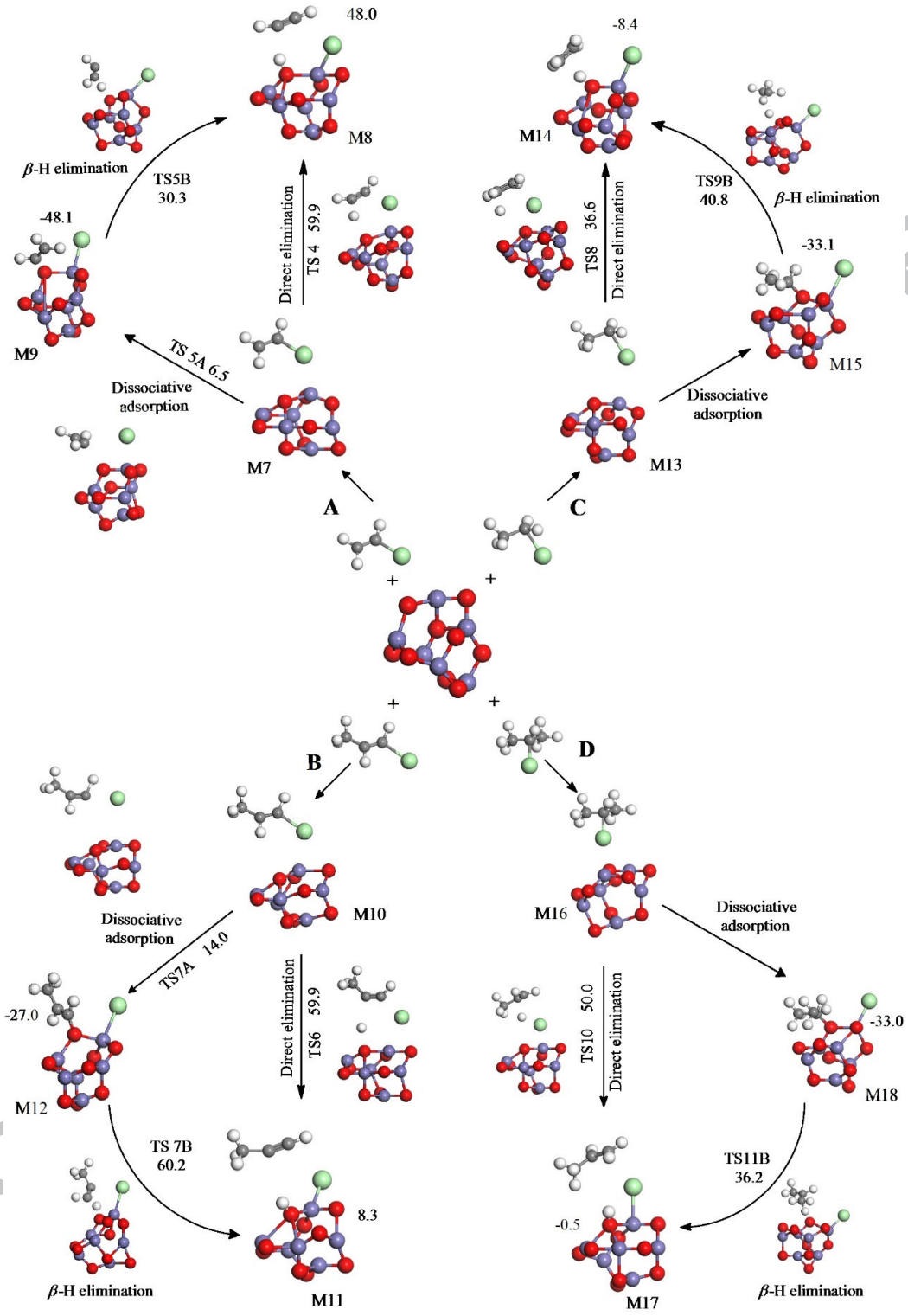

Figure 5: Reaction of Chloroethene (A), 1-Chloro-1-propene (B) Chloroethane (C), and 2-Chloropropane (D) with the Hematite (α-Fe_2O_3) cluster. Values are in kcal mol^{-1} in reference to the physisorbed M7, M10, M13, M16 structures; respectively.

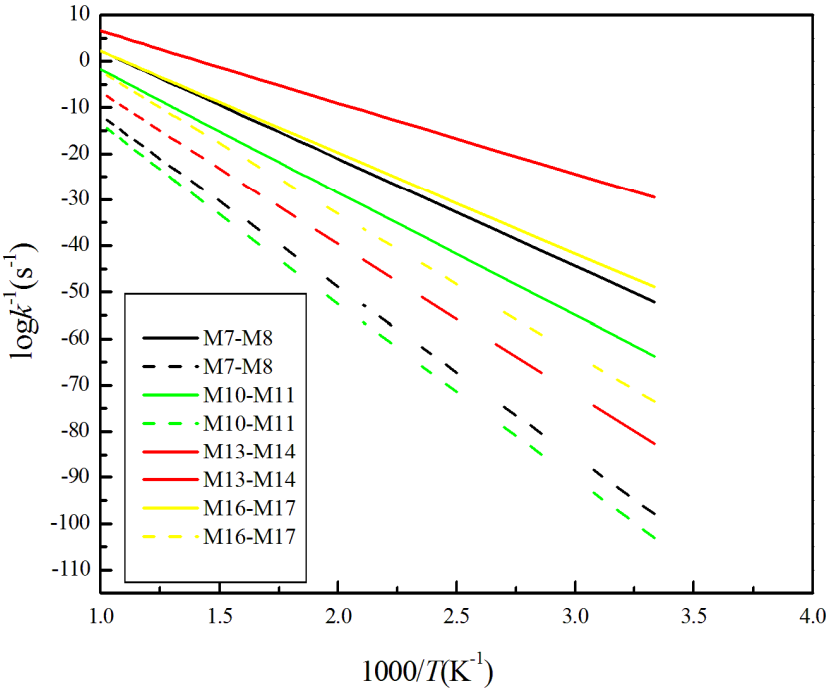

Figure 6: Variation of the reactions rates with temperatures for the elimination (solid line) and dissociative addition (dashed line) pathways**.**

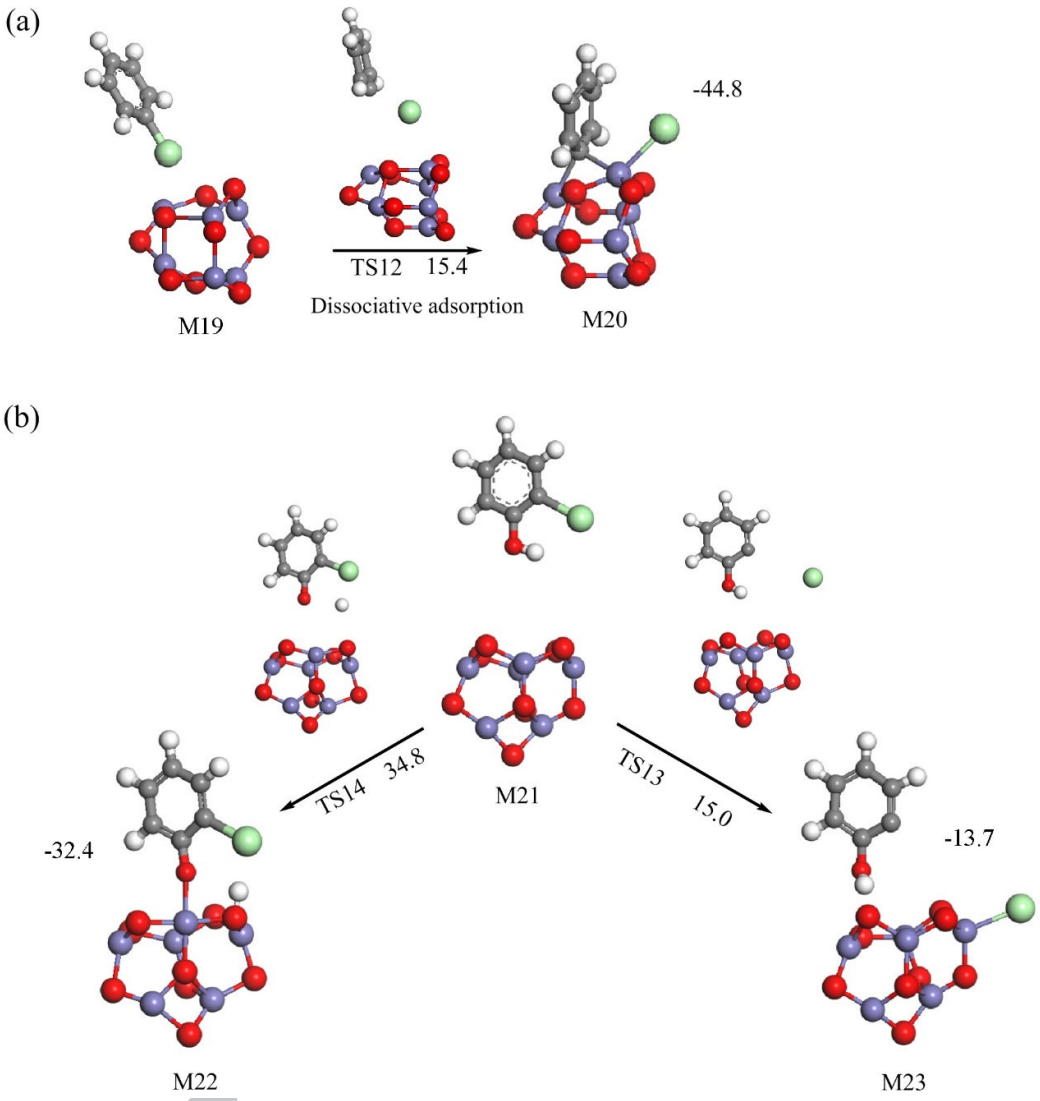

Figure 7: Reaction of chlorobenzene (a) and 2-chlorophenol (b) with Hematite (α-Fe_2O_3) cluster. Values are in kcal mol^{-1} in reference to the initial reactants.

Highlights

- Reactions of HCl and chlorinated VOCs with iron (III) oxide have been analysed.
- Successive dissociation of HCl on F-O bonds converts Fe_2O_3 into iron chloride.
- Decomposition of chlorinated VOCs mainly occurs by dissociative addition.
- Results herein demonstrate the chlorine fixation ability of iron oxides.